Journal of Geophysical Research: Space Physics

TECHNICAL REPORTS: METHODS

10.1002/2017JA024543

Key Points:
- An improved technique for determining the global ionospheric convection using SuperDARN measurements is described
- Our model is based on a set of state descriptors using a minimum of assumption
- The fill-in convection model is determined from all historic SuperDARN database and principal component regression

Correspondence to:
J. W. Gjerloev,
jesper.gjerloev@jhuapl.edu

Citation:
Gjerloev, J. W., Waters, C. L., & Barnes, R. J. (2018). Deriving global convection maps from SuperDARN measurements. *Journal of Geophysical Research: Space Physics*, *123*. https://doi.org/10.1002/2017JA024543

Received 30 JUN 2017
Accepted 9 MAR 2018
Accepted article online 12 MAR 2018

Deriving Global Convection Maps From SuperDARN Measurements

J. W. Gjerloev[1,2], C. L. Waters[3], and R. J. Barnes[1]

[1]Applied Physics Laboratory, The Johns Hopkins University, Laurel, MD, USA, [2]Birkeland Center, University of Bergen, Bergen, Norway, [3]School of Mathematical and Physical Sciences, University of Newcastle, Newcastle, New South Wales, Australia

Abstract A new statistical modeling technique for determining the global ionospheric convection is described. The principal component regression (PCR)-based technique is based on Super Dual Auroral Radar Network (SuperDARN) observations and is an advanced version of the PCR technique that Waters et al. (2015, https//:doi.org.10.1002/2015JA021596) used for the SuperMAG data. While SuperMAG ground magnetic field perturbations are vector measurements, SuperDARN provides line-of-sight measurements of the ionospheric convection flow. Each line-of-sight flow has a known azimuth (or direction), which must be converted into the actual vector flow. However, the component perpendicular to the azimuth direction is unknown. Our method uses historical data from the SuperDARN database and PCR to determine a fill-in model convection distribution for any given universal time. The fill-in data process is driven by a list of state descriptors (magnetic indices and the solar zenith angle). The final solution is then derived from a spherical cap harmonic fit to the SuperDARN measurements and the fill-in model. When compared with the standard SuperDARN fill-in model, we find that our fill-in model provides improved solutions, and the final solutions are in better agreement with the SuperDARN measurements. Our solutions are far less dynamic than the standard SuperDARN solutions, which we interpret as being due to a lack of magnetosphere-ionosphere inertia and communication delays in the standard SuperDARN technique while it is inherently included in our approach. Rather, we argue that the magnetosphere-ionosphere system has inertia that prevents the global convection from changing abruptly in response to an interplanetary magnetic field change.

Plain Language Summary The ionospheric convection is one of the fundamental electrodynamic physical parameters associated with the Earth interactions with space. In this paper we outline a fundamentally new technique for determining the global ionospheric convection. The principal component regression-based technique is based on Super Dual Auroral Radar Network (SuperDARN) observations and is an advanced version of the principal component regression technique that Waters et al. (2015, https//:doi.org.10.1002/2015JA021596) used for the SuperMAG data. Our method uses all historical data from the SuperDARN database and principal component regression to determine a fill-in model convection distribution for any given universal time. The fill-in data process is driven by a list of state descriptors (magnetic indices and the solar zenith angle), and the final solution is then derived from a fit to the SuperDARN measurements and the fill-in model. When compared with the standard technique, we find that our provides improved solutions.

1. Introduction

Over the last two decades the Super Dual Auroral Radar Network (SuperDARN) collaboration (e.g., Chisham et al., 2007; Greenwald et al., 1985) has provided the primary source for measurements of the large-scale ionospheric convection. The network of high-frequency radars provides line-of-sight (LOS) Doppler velocity measurements. Currently, 23 radars are operational in the northern hemisphere and 12 in the southern hemisphere. Each has a wide field of view of ~50°. In standard configuration, backscatter is received from 16 beams each with some 75 range gates. Each radar provides a full field-of-view scan with a temporal resolution of 1–2 min and the typical spatial resolution for a given range gate of 45 km in the LOS direction.

While this system has the capability of providing continuous and global coverage of ionospheric convection, there are two inherent complications: sparse and variable spatial coverage and LOS measurements (not full vector flows). Most studies are interested in the characteristics of the flows and not the LOS flow for a given beam direction. Thus, the LOS velocity measurements need to be used to derive a global convection pattern, which then provides the scientific data product to the research community. This is a nontrivial challenge that has been discussed in many papers (e.g., Fiori et al., 2010; Ruohoniemi & Baker, 1998; Ruohoniemi & Greenwald,

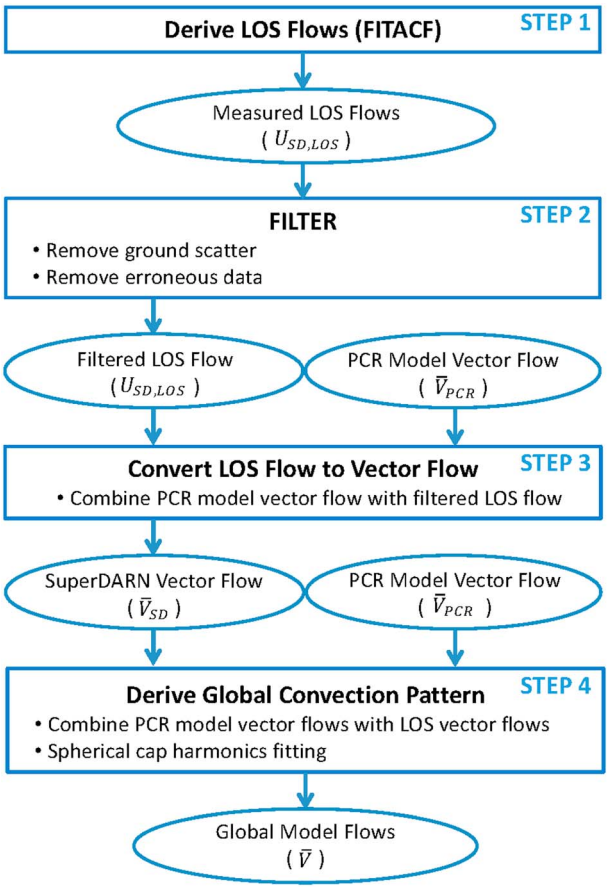

Figure 1. Flow chart showing the basic steps in deriving the global convection pattern (see text for discussion).

1995, 1996, 2005; Shepherd & Ruohoniemi, 2000). The standard SuperDARN data processing uses an interplanetary magnetic field (IMF)-driven, fill-in data model, which combined with the measured LOS flows allows a basis function fit. The purpose of the fill-in data model is to provide data in regions of sparse or no measurements to ensure that the basis function solution is constrained. The impact of the original fill-in model on the magnetosphere-ionosphere (M-I) community cannot be overstated, and the solutions have been utilized in a vast number of studies and applications.

The question is how such a fill-in model should be derived. The present algorithm was developed from the initial work of Ruohoniemi and Baker (1998) and advanced by Shepherd and Ruohoniemi (2000). The original work was based on measurements from a single radar, which was organized by the IMF magnitude and orientation. Discrete bins were defined (e.g., positive IMF B_y and positive IMF B_z), and global average potential distributions were derived for each bin. For a given event the IMF conditions define which fill-in model should be combined with the measured LOS. This approach has been refined (e.g., Cousins & Shepherd, 2010; Ruohoniemi & Greenwald, 2005) using data from more radars and more IMF bins. However, the fundamental assumption remains; that is, there is a causal relationship between the IMF and the ionospheric convection. Global solutions based on principal component analysis (e.g., Cousins, Matsuo, & Richmond, 2013; Grocott et al., 2012; Kim et al., 2012) have been derived although it should be noted that Cousins et al. (2013) found that using all 30 modes only explained 77% of the variance.

The vast majority of past studies have utilized IMF to organize the data. This implies a cause-and-effect approach where the solar wind is the cause and the ionospheric convection is the effect. Such an approach is complicated by several inherent complications (discussed in section 4.2) none of which are trivial. We have chosen to use a fundamentally different approach that does not include IMF and thus is not subject to these complications.

The purpose of this paper is to use the sparse SuperDARN LOS measurements to provide global solutions of the convection electric field. As a secondary purpose, the solutions are compared with those currently provided by the SuperDARN community (through the Virginial Tech website, http://superdarn.org/tiki-index.php) and argue that our technique provides improved solutions. Section 2 outlines the SuperDARN technique, section 3 describes the multilinear-regression technique we use to derive the fill-in data, section 4 is the discussion and validation, and finally, we summarize and list our conclusions in section 5.

2. Deriving the Global Convection Pattern

The basic problem with the measurements provided by the SuperDARN high-frequency radars is converting the sparse nonuniformly distributed line-of-sight flows (one vector velocity component) to global convection patterns on minute time and ~1–2° spatial scales. The SuperDARN software developed over the last few decades consists of the FITACF routine that calculates the measured LOS flows, filtering aimed at removing ground scatter and erroneous LOS flows, and finally, a software package that derives the ionospheric convection distribution from the filtered LOS flows. In our technique the global convection is derived in four basic steps as illustrated in Figure 1.

Step 1: Obtain LOS velocity measurements.

Step 2: Filter LOS measurements.

Step 3: Convert LOS measurements to vector flows.

Step 4: Derive the global convection pattern.

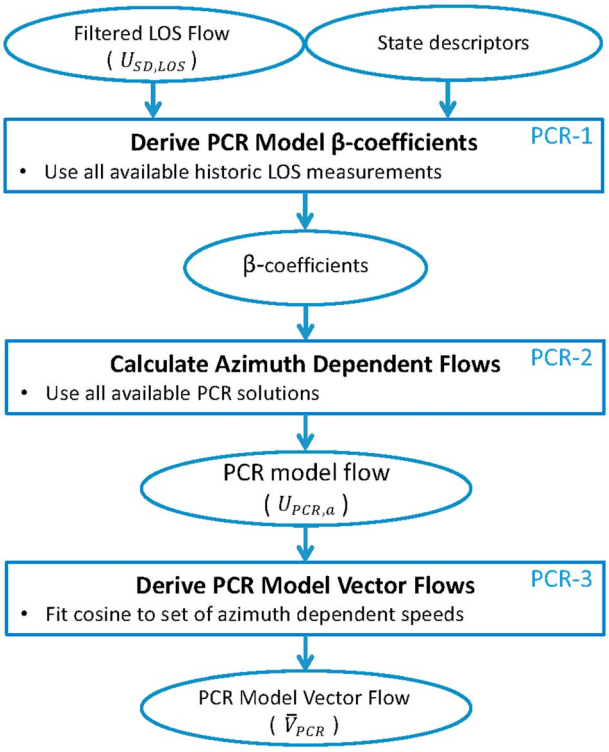

Figure 2. Flow chart showing the basic steps in deriving the principal component regression (PCR) model vector flows (see text for discussion).

The focus of the present paper is steps 3 and 4. Step 1 has been examined by Ponomarenko and Waters (2006), who described a list of recommended improvements to the FITACF data processing package (we have used version 5.0). Step 2 involves the identification of backscatter type and location and is briefly discussed below. Steps 3 and 4 are completely different from previous SuperDARN techniques and are given a more thorough description below in Figure 2.

2.1. STEP 1: Obtain LOS Velocity Measurements

The FITACF software package derives the LOS flows from the autocorrelation function of the backscattered radar signals, for each range gate of each beam of every radar. This set of routines provides the LOS Doppler velocity, spectral width, and signal-to-noise ratio. Ponomarenko and Waters (2006) discussed improvements to this technique, and we refer to that paper for a thorough discussion of how the LOS flows are derived and estimate of the uncertainties. In this paper we simply use the LOS data provided by the FITACF routines.

2.2. STEP 2: Filter LOS Measurements

The LOS velocity measurements provided by FITACF may be divided into three categories: (i) ionospheric convection, (ii) ground scatter, and (iii) erroneous data.

In order to derive the ionosphere convection, erroneous data and ground scatter must be removed. We have not addressed this problem and instead accepted the standard SuperDARN filtering technique. The revised model is thus derived from the same set of LOS measurements that is used for the standard SuperDARN models released by Virginia Tech (http://superdarn.org/tiki-index.php).

Several attempts have been made to identify ground scatter, and currently, the SuperDARN data include a ground scatter identifier flag that is intended to identify measurements that are due to ground scatter. The process is illustrated in Figure 6 of Ponomarenko et al. (2007). For the present, this flag is used to exclude ground backscatter. Poor quality backscatter with large uncertainties is also excluded using the error estimates provided by the FITACF SuperDARN software.

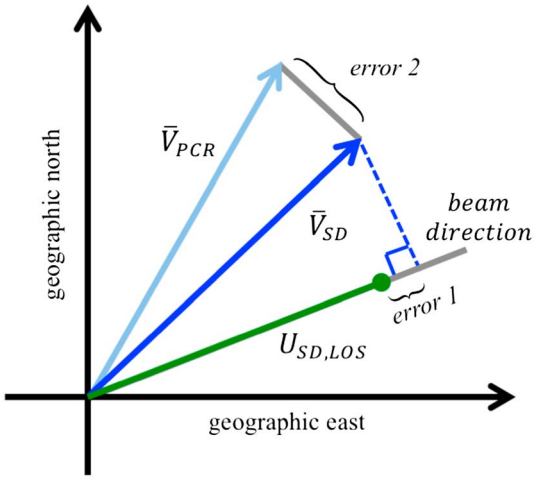

Figure 3. We derive the vector flows ($\overline{V}_{SD}$) using a weighted fitting to the vector fill-in flow ($\overline{V}_{PCR}$) and the Super Dual Auroral Radar Network measured line-of-sight (LOS) speed ($U_{SD,\ LOS}$). We minimize the sum of the two errors while weighting error 1 higher than error 2 (the Curvefit routine is used, and error 1 is given a weight of 3).

2.3. STEP 3: Convert LOS Measurements to Vector Flows

The procedure for converting the measured LOS flows to vector flows was reviewed and is different to the SuperDARN technique (Ruohoniemi & Baker, 1998; Ruohoniemi & Greenwald, 1996) currently made available from Virginia Tech (http://superdarn.org/tiki-index.php). The measured LOS flows are combined with the fill-in vector flow (see section 3 for an explanation of how these flows are derived) to obtain a best fit solution to the vector flow. This is similar to the method used by Ruohoniemi and Greenwald (1995, 1996). For the revised algorithm, the vector flows ($\overline{V}_{SD}$) are derived from a weighted fit to the vector fill-in flow (VPCR, see Figure 2 and section 3) ($\overline{V}_{PCR}$) and the SuperDARN measured LOS flows ($U_{SD,\ LOS}$) by minimizing the error between the resulting vector flow, $\overline{V}_{SD}$, and the inputs $U_{SD,\ LOS}$ and $\overline{V}_{PCR}$:

$$\text{error} = \left|U_{SD,LOS} - \overline{V}_{SD}\cdot\hat{k}_a\right| + \left|\overline{V}_{PCR} - \overline{V}_{SD}\right| \quad (1)$$

where $\hat{k}_a$ is the unit vector in the beam direction (azimuth). The standard gradient-expansion algorithm provided by IDL, "Curvefit" (Marquardt, 1963), was used to compute a nonlinear least squares fit and weight the error toward the actual measurement, $U_{SD,\ LOS}$, using a factor of 3.

A higher factor minimizes $\left|U_{SD,LOS} - \overline{V}_{SD}\cdot\widehat{k}_a\right|$, while a lower factor minimizes $\left|\overline{V}_{PCR} - \overline{V}_{SD}\right|$. The value 3 was carefully chosen by evaluating probability density distributions of the two terms on the right side of equation (1) as a function of the weight factor.

One of the advantages of this approach is that any number of flow vectors and LOS flows can be combined and any appropriate weights can be assigned to the input data. Further, it is computationally efficient.

2.4. STEP 4: Derive the Global Convection Pattern

With the measured LOS flows filtered and converted to vector flows, the problem is to derive the global convection pattern from the sparse nonuniformly distributed measurements. Furthermore, the number of LOS flows varies wildly over time and large spatial regions may be without any measurements. These complications must be addressed in order to derive the global convection pattern. In line with previous SuperDARN models, this is achieved by combining the measurements with fill-in data. The procedure for obtaining these fill-in data is different from the present SuperDARN technique.

Our technique is an advanced version of the multilinear regression approach that Waters et al. (2015) used for the SuperMAG data (Gjerloev, 2012). In applying that technique to SuperDARN data we are faced with several complications: (1) SuperDARN provides LOS flows, while SuperMAG provides vector measurements; (2) SuperDARN requires significant filtering of the LOS flows to remove ground scatter and erroneous data; (3) the locations of SuperDARN measurements are constantly changing, while SuperMAG provides long uninterrupted time series; and (4) SuperDARN location of backscatter is ambiguous, while SuperMAG observations are from well-known fixed locations. These differences (in particular the first) require some nontrivial changes from the technique published by Waters et al. (2015).

Finally, we should mention that while it seems reasonable to use magnetic indices to derive ground-level magnetic field perturbation, it is not as obvious that those same indices also provide a means to derive ionospheric convection.

2.4.1. Combining Measured LOS and Model Flows

In order to derive the final solution, spherical cap harmonics are fitted to the derived SuperDARN vector flows $\overline{V}_{SD}$ and the fill-in vector flows $\overline{V}_{PCR}$. The main purpose of the fill-in flows is to constrain the spherical cap harmonics solution (Haines, 1985). If sufficient LOS measurements were available and if these were more or less uniformly distributed, there would be no need for the fill-in vector flows. As described in section 2.3 a secondary purpose of the fill-in model is to convert the LOS flows to vector flows.

The fill-in model is thus used twice: first to derive vector flows, $\overline{V}_{SD}$, and second to derive global solutions (see Figure 1). To ensure that the final solution is measurement driven, the $\overline{V}_{SD}$ are weighted higher than the model-derived $\overline{V}_{PCR}$. This was ensured by evaluating the two terms (see Figure 3):

$$\left|\overline{V}_{PCR} - \overline{V}_{SD}\right| \text{ and } \left|U_{SD,LOS} - \overline{V}_{SD}\cdot\widehat{k}_{a.}\right|$$

for a list of weights ranging from 1 to 10. A higher weighting will minimize the second term, while a lower weighting will minimize the first term. Calculating solutions for a full day allow us to derive the distribution of these two terms. The choice of 3 was made since the second term is then in agreement with expected measurement uncertainty.

Furthermore, the fill-in vectors are deleted if they are within 100 km of a measurement. The actual spatial resolution of the SuperDARN measurements are typically stated as 40–50 km although this is complicated by a list of factors (e.g., deviation between the actual propagation from the assumed straight line) as well as the smearing caused by the median filtering (see section 4.4).

Finally, it should be noted that our technique does not require this final spherical harmonic fit. If a gridded solution is sufficient for an investigation, then there is no need to perform the spherical harmonic fit.

3. Deriving the Fill-in PCR Model

The fill-in data are obtained using a principal component regression (PCR) approach, similar to that described for SuperMAG data by Waters et al. (2015). However, for SuperDARN data, the location of the

Table 1
List of State Descriptors Used to Derive the Fill-in Model

Parameter	Explanation
$SML_{D,S}$	SML (SuperMAG equivalent of AL) derived from stations located under the dark and sunlit ionosphere, respectively
$SMU_{D,S}$	SMU (SuperMAG equivalent of AU) derived from stations located under the dark and sunlit ionosphere, respectively
$SMR-LT$	SMR (SuperMAG equivalent of SYM-H) derived from stations located in four local time regions
$SYM-D$	Longitudinally symmetric (SYM) disturbance index for D-component
$ASY-D,H$	Longitudinally asymmetric (ASY) disturbance index for D- and H-component
SZA	Solar zenith angle

Note. Some are SuperMAG versions of the IAGA approved indices and others are IAGA approved indices.

LOS velocity measurements and the component of the actual flow changes. Therefore, additional steps are required, compared with the SuperMAG method. The main difference is that for SuperMAG data, we determine multilinear solutions to two components (geographic north and east), while for SuperDARN, we fit to 36 azimuth components covering the 360°, and the vector is then determined by a cosine fit to these 36 solutions.

The fill-in velocity data are derived independent of any IMF data, as follows:

PCR-1 Derive PCR model β-coefficients.
PCR-2 Calculate azimuth-dependent flows.
PCR-3 Derive PCR model vector flows.

These three basic steps are illustrated in Figure 2.

3.1. PCR-1: Derive PCR Model β-Coefficients

The coefficients are derived from historic filtered SuperDARN measurements. All the LOS flow measurements obtained over 1994–2017 from the northern hemisphere are binned by an equal area magnetic latitude (MLAT)-magnetic local time (MLT) grid (Ruohoniemi & Greenwald, 1996) in addition to the azimuth of the radar beam azimuth. The Altitude Adjusted Corrected Geomagnetic (AACGM) coordinates (Baker & Wing, 1989) were used for the spatial organization or binning of the LOS measurement, but it is important to note that the azimuth directions for the LOS measurements are in geographic coordinates. All vectors and basis function calculations are thus completed in an orthogonal coordinate system (see section 4.3.1 for a discussion of this problem).

The regression model is given by

$$U_{\mathrm{PCR,a}} = \beta_0 + \beta_1 P_1 + \ldots + \beta_k P_k + \epsilon \tag{2}$$

where $U_{\mathrm{PCR,\,a}}$ are the fitted velocity components at a given MLT, MLat, and azimuth (a) which is given by the radar beam orientation; the P_k are eigenvectors of the covariance matrix derived from the magnetic indices and solar zenith angle (SZA) values that represent the independent variables; β_k are the regression coefficients; and ϵ are the model errors assumed to have zero mean.

The β_k are derived from all northern hemisphere historic LOS measurements. We derive the coefficients for each radar, beam, and range gate (here referred to as an ID). For each LOS measurement we know the position and azimuth as well as the list of eigenvectors, P_k. With the current number of SuperDARN radars, the number of contributing range gates ($U_{\mathrm{PCR,\,a}}$ solutions) at a given azimuth varies between zero and 20. For a given MLT and MLat bin we thus get a fairly large number of $U_{\mathrm{PCR,\,a}}$ solutions, which then has the distinct advantage that we can determine to what extent a particular ID is statistically in agreement with all other contributions. In other words, an objective quality evaluation of all ID's can be made. In addition, this also provides some robustness to the subsequent fitting (PCR-3; section 3.3).

The result is a very large set of β coefficients that are determined from the complete set of historic northern hemisphere (filtered) LOS measurements:

$$\beta = \beta(\mathrm{MLT}, \mathrm{MLat}, \mathrm{azimuth}, \mathrm{ID}) \tag{3}$$

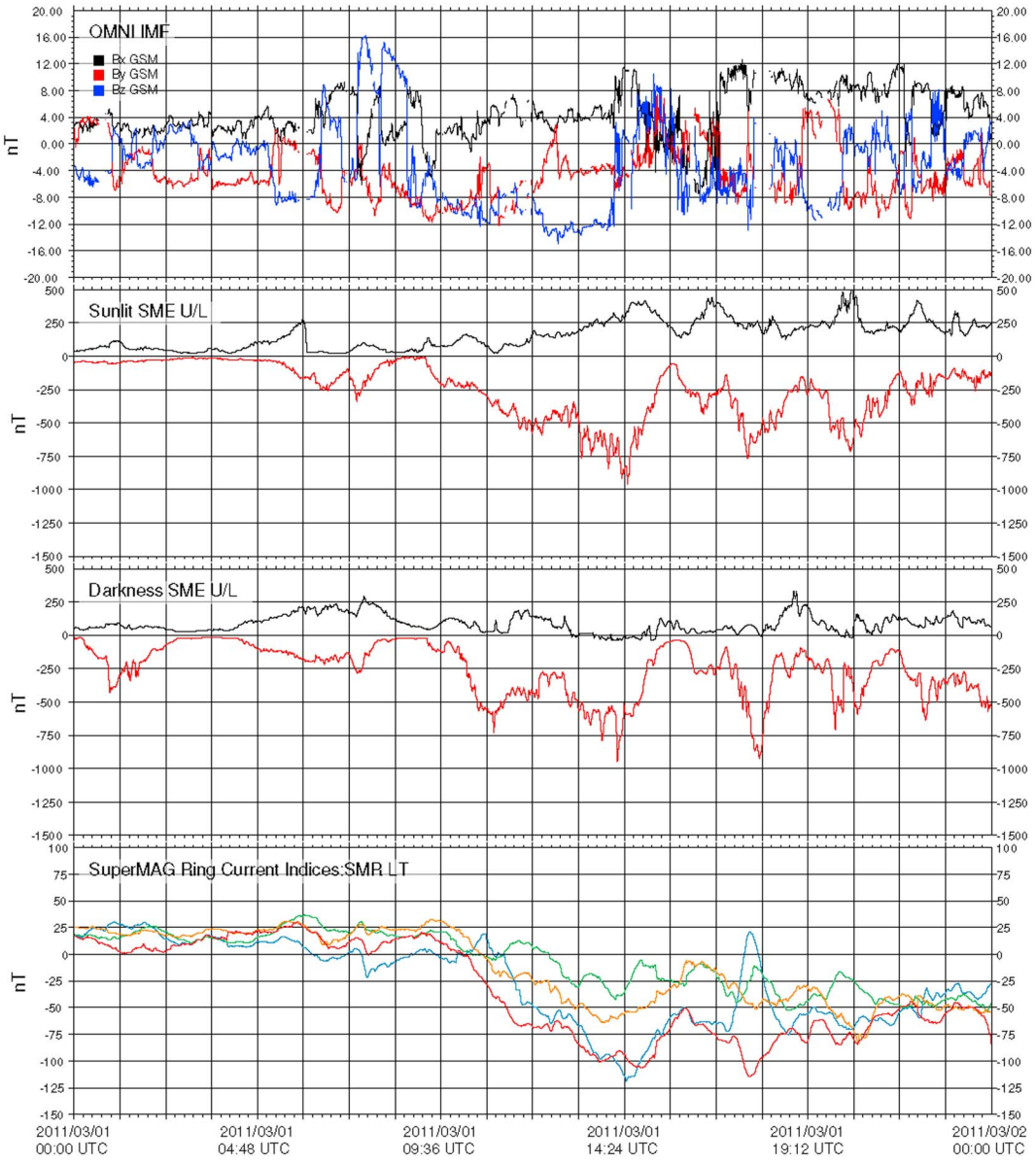

Figure 4. 1 March 2011 used to derive the statistics. Panels from top to bottom: OMNI IMF data, SuperMAG sunlit SML/SMU, SuperMAG darkness SML/SMU, and SuperMAG SMR-LT.

The drivers or state descriptors, P_k, used to derive $U_{PCR,\,a}$ were chosen to be the same set of parameters that were shown to work for the SuperMAG initiative (see Table 1). These are a subset of the list used by Waters et al. (2015) (and is identical to the list actually used by the SuperMAG collaboration http://supermag.jhuapl.edu) and are only a function of time:

$$P_k = P_k(\mathrm{UT}) \tag{4}$$

where P_k are selected from the list of SuperMAG derived indices (Gjerloev et al., 2010; Newell & Gjerloev, 2011, 2012) and SZA. The SuperMAG indices are derived from all available ground-based magnetometers, and some of them can be seen as extensions of well-known magnetic indices (e.g., SML is the SuperMAG version of AL). Note that no solar wind parameters are involved and the reasons for this are discussed in section 4.2.

The β coefficients are determined using PCR where the LOS measurements are regressed onto a set of eigenvectors derived from the covariance matrix. Finally, it should be noted that the β-coefficients needs to be determined only once.

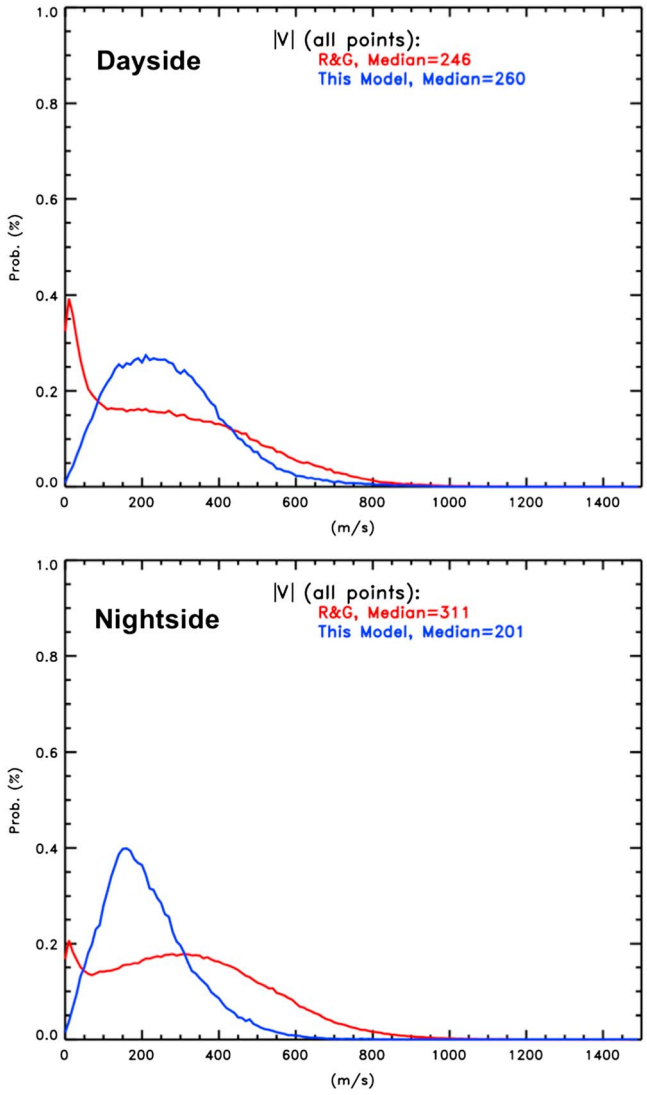

Figure 5. Speed. (top) Probability density function for final solution on the dayside (06 to 18 magnetic local time) for the R&G model (red) and this model (blue). (bottom) Same as top but for nightside.

3.2. PCR-2: Determine Azimuth Dependent Flows

For a given universal time (UT) the state descriptors, P_a, are used as input into equation (2), which along with all the predetermined β coefficients (determined in PCR-1) in principle allow us to calculate the velocity components for each of the ID's. For each spatial bin (MLT, MLat) a fairly large number of independent $U_{PCR,\,a}$ solutions are thus obtained. Each of these can be interpreted as vector components in the $\hat{k}_a$ direction. Below we explain how this set of flow components is used to derive the model vector flow.

3.3. PCR-3: Derive PCR Model Vector Flows

With the MLT-MLat-azimuth velocity component solutions, $U_{PCR,\,a}$, determined in sections 3.1 and 3.2, the fill-in vector flows at a given MLT and MLat and UT may be derived.

A velocity component, $U_{PCR,\,a}$, and the flow vector, $\overline{V}_{PCR}$, is related by

$$U_{PCR,a} = \overline{V}_{PCR} \cdot \hat{k}_a \tag{5}$$

where $\hat{k}_a$ is the unit vector in the beam direction (azimuth). The fill-in or PCR vector flow was obtained from a cosine function fit to all $U_{PCR,\,a}$ solutions. The flow magnitude is found from the amplitude of the cosine fit, and the phase provides the direction of the flow. SuperDARN does not cover all azimuths at all MLT-MLat bins but does typically cover a fairly large range of azimuths. Furthermore, the technique yields a large number of individual $U_{PCR,\,a}$ solutions. This provides much needed robustness to the fit and thus the flow vector, $\overline{V}_{PCR}$. We organize the $U_{PCR,\,a}$ solutions in 36 azimuth bins of each 10° width and determine the median flow at that azimuth. In reality SuperDARN may not provide sufficient azimuth coverage and/or solutions to ensure a meaningful flow vector, $\overline{V}_{PCR}$, for a given MLT, MLat, and UT. We thus require the $U_{PCR,\,a}$ solutions to cover an azimuth range of less than 45° and include more than 10 solutions.

4. Discussion

When proposing a new approach to deriving a SuperDARN convection model, the basic question is as follows: To what extent is the new better than the past models? Addressing this hinges on the presence of definitive or ground-truth convection distributions. Comparing with space borne (e.g., Defense Meteorological Satellite Program velocity meter) or ground-based instruments (e.g., Incoherent Scatter Radars) is not trivial. Among many other complications there are significant differences in the spatial and temporal resolutions of SuperDARN and these measurements. For now, in order to avoid complications in arguing for the validity of another data set, validation of the proposed method is solely based on the SuperDARN LOS measurements. An independent comparison with other convection electric field measurements will be performed in a follow-up paper.

4.1. Model Performance

4.1.1. Quantifying Differences Between Our Model and the Standard SuperDARN Model

Results from the new approach described in this paper, the measured LOS flows and the convection model provided by the SuperDARN Web service (http://superdarn.org/tiki-index.php) were compared. The existing data available from the SuperDARN Web service are based on the technique discussed by Ruohoniemi and Greenwald (1996) and Ruohoniemi and Baker (1998), hereafter referred to as RG&RB.

When comparing the solutions made available at the above mentioned website, it is important to point out that they are based on the same set of measured LOS flows since we have made no changes to steps 1 and 2 described in section 2.

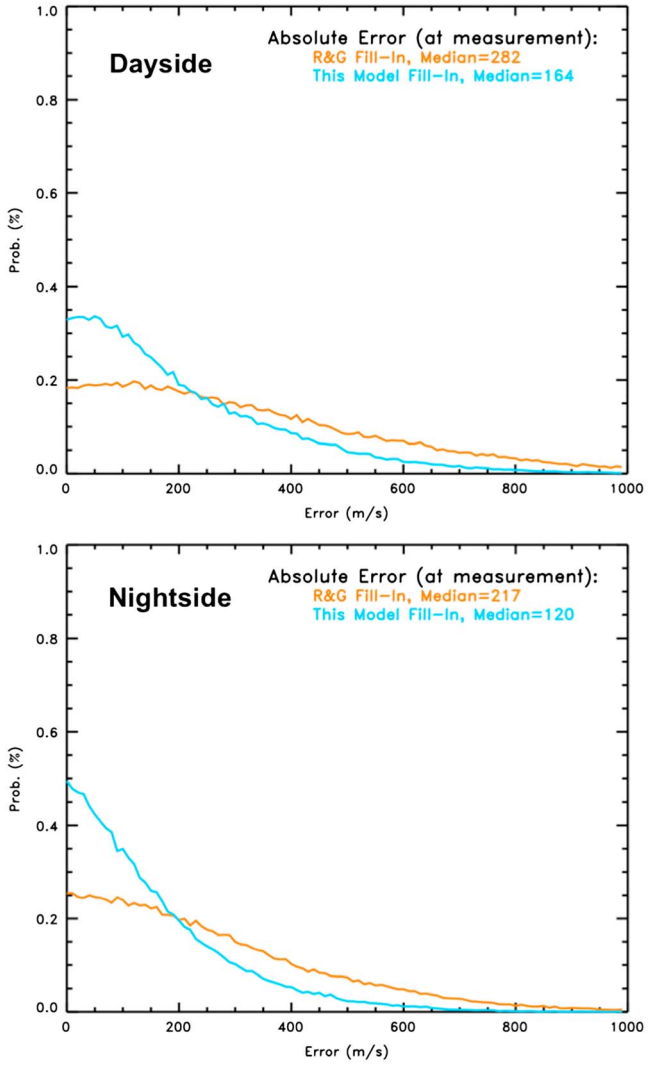

Figure 6. Absolute error between the fill-in model and the measured line-of-sight velocity components. (top) Probability density function for absolute error on the dayside (06 to 18 magnetic local time) for the R&G model (orange) and this model (light blue). (bottom) Same as top but for nightside.

Figure 4 shows the OMNI IMF conditions and a list of magnetic indices for one full day. The second and third panels show the SuperMAG SML and SMU (SuperMAG equivalent of AL and AU; Newell & Gjerloev, 2011) for the sunlit and darkness ionosphere, respectively (Gjerloev et al., 2010). The fourth panel shows the SuperMAG partial ring current indices (Newell & Gjerloev, 2012). The IMF was variable with long periods of southward B_z and the magnetosphere responded by developing a considerable ring current reaching some −120 nT. The auroral electrojets show a string of intensifications, some reaching −1,000 nT. Note the difference between the sunlit electrojet activity and the darkness electrojet activity, which is information used to derive the PCR model (see section 3).

A day provides a total of 720 gridded distributions of the vector flow (or the electric potential), which along with the measured LOS flows provides the statistical basis for comparing the methods. We calculated the statistics for 10 additional moderately disturbed days covering different seasons and found them to be in agreement with this representative day.

Figure 5 shows probability density functions (PDFs) of the flow magnitude for the solutions for the dayside (top) and nightside (bottom). The most striking difference between the two techniques is the shape. While the new PCR-based model shows a single maximum and a shape similar to a Maxwell-Boltzmann distribution, the RG&RB solutions show a double-peak distribution. Because of this difference in shape, it is difficult to compare the median values. However, in general, the magnitudes do not appear to differ by much. The PCR-based model nightside solutions appear to have slightly smaller flows than the dayside, while the RG&RB model shows the opposite.

The above differences may be due to differences in the fill-in solutions obtained from the two techniques. Figure 6 shows the difference between the measured LOS flows and the fill-in vector flows projected onto the beam azimuth (equation (5)). Recall that both data fill-in models do not use actual SuperDARN measurements and are derived from either IMF (RG&RB) or magnetic indices/SZA (PCR-based). As Figure 6 shows the PCR-based solution produces flows that have significantly better agreement with the measurements compared with the RG&RB model. This is the case on both the dayside and nightside, which provides a very strong argument for the validity of our technique.

While the PCR-based model agreement with the measurements is an important parameter, the fundamental question is how well the final solutions agree with the measured LOS flows. As seen in Figure 7 the new PCR-based model is slightly better on the dayside and significantly better on the nightside.

One problem with the comparison made in Figure 7 is that it is based on a circular argument where the measured LOS flows are used to derive the final model and then the final model is compared with those same measured LOS flows. In order to avoid this all measurements in a 2 hr wide MLT wedge centered at midnight and at noon were deleted. Any measurement within this wedge was not used in the derivation of the final solutions. The final solutions using the modified data set were compared with the measurements within each of those wedges. Figure 8 shows the error, and we find that the two models perform in a similar way within the dayside wedge. However, for the nightside wedge the new PCR-based model is significantly better. Given the results from Figure 6, we argue that the wider the gap in SuperDARN measurements, the better the PCR-based model will perform, relative to the existing RG&RB model.

Finally, we plot the PDF of the temporal variations for the final solutions. This provides a measure of the performance of accurately representing the temporal development of ionospheric convection. The underlying assumptions for the two techniques are fundamentally different (see section 4.2 for a discussion), and we thus expected differences in the temporal variation of the final spatial maps obtained from the two

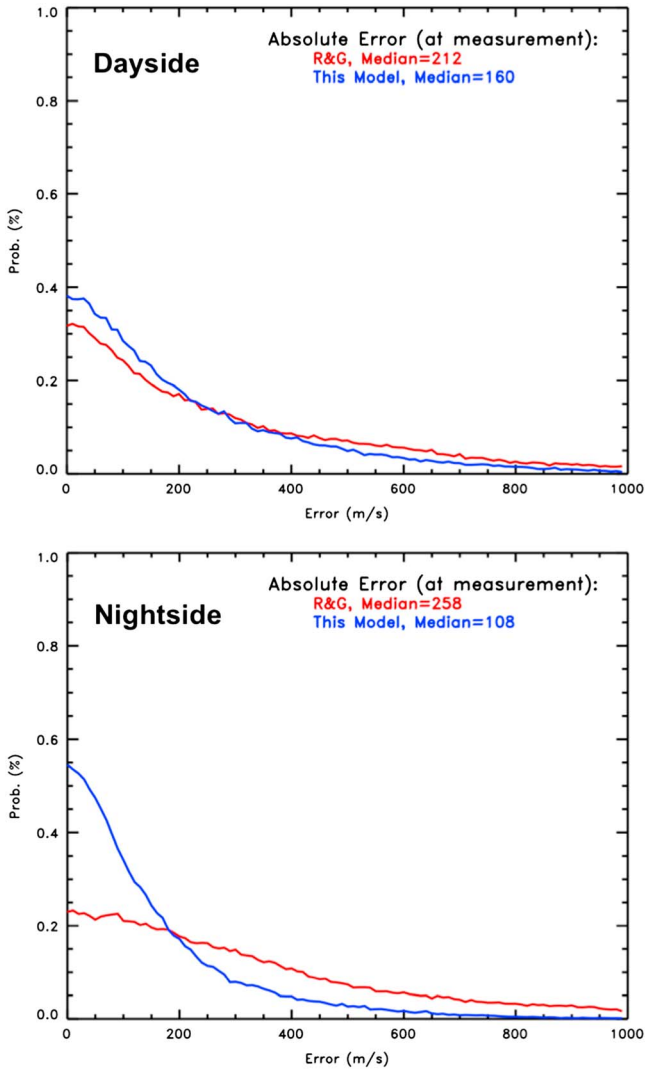

Figure 7. Absolute error between the final solution and the measured line-of-sight velocity components. (top) Probability density function for absolute error on the dayside (06 to 18 magnetic local time) for the R&G model (red) and this model (blue). (bottom) Same as top but for nightside.

models. As was the case for the magnitude of the velocity components seen in Figure 6 we find that the variability of the flows in the two models differ (Figure 9). The RG&RB model shows an extended tail indicating a highly dynamic solution, while our distribution again shows similarities to a Maxwell–Boltzmann distribution.

4.1.2. Model Performance.

Figure 10 shows an example that illustrates the difference in the convection distribution resulting from the two different techniques. This example is chosen to illustrate the impact of the fill-in model and the IMF dependence in the RG&RB model and thus occur during a change in the IMF orientation. The purpose of the figure is simply to illustrate the response of the two models to a change in IMF. In the RG&RB solution the convection changes rather abruptly. Both direction and magnitude change, and the polar cap potential drops by about 50% in just 2 min. In our model we do not see any noticeable change despite the fact that we use the same set of measured LOS flows. This difference in temporal behavior is reflected in the PDFs shown in Figure 9 where our model is far less dynamic. In section 4.2.3 we further discuss the fundamental difference in temporal behavior between the two techniques.

Near noon at 62° MLat we see a few flow vectors in our model that appear to be driven purely by the fill-in model. This is likely artifacts. The problem is seen in equations (2) and (3) that in cases of poor statistics may not lead to robust β solutions. The poor statistics is an issue at low latitudes where the flows are weak and thus often flagged as ground scatter, little back scatter and, finally, only a few radars provide coverage. This problem can be solved with an improved ground scatter identification technique, additional future observations, and/or some spatial filtering.

This example illustrates the difficulties of deriving the global convection. In this case it is not possible to objectively determine to what extent each model is in agreement with the actual convection electric field since we have no ground truth for comparison. The examples are not a replacement for statistical results shown in Figures 5–9.

4.2. Modeling Approach

Previous and current SuperDARN fill-in data models have been based on SuperDARN measurement categorized by some sort of IMF binning. In contrast, our PCR-based model uses what we refer to as state descriptors. Waters et al. (2015) briefly discussed the inherent assumptions associated with an IMF driven model approach. The application to the SuperDARN data and assumptions associated with our approach are discussed below.

4.2.1. IMF Driven Fill-in Model

An IMF-driven model is essentially a cause-and-effect model in which the IMF is the cause and the ionospheric convection is the effect. Such an approach is based on a series of fundamental assumptions:

1. The delay between the driver (front side of magnetosphere) and the effect (ionospheric flows) is known.
2. The M-I system has no inertia.
3. The history of the solar wind-M-I system is irrelevant.
4. Internal M-I processes are irrelevant.
5. The measured solar wind conditions actually interact with the magnetospheric field, and the propagation delay between measurement and magnetopause is known.

Consider a scenario where measurements of the driver (here IMF) show constant conditions except for a single spike. Without accounting for delays (A) and the inertia of the M-I system (B), the convection distribution will instantaneously change to the new state and then back to the previous state. A cause-and-effect model

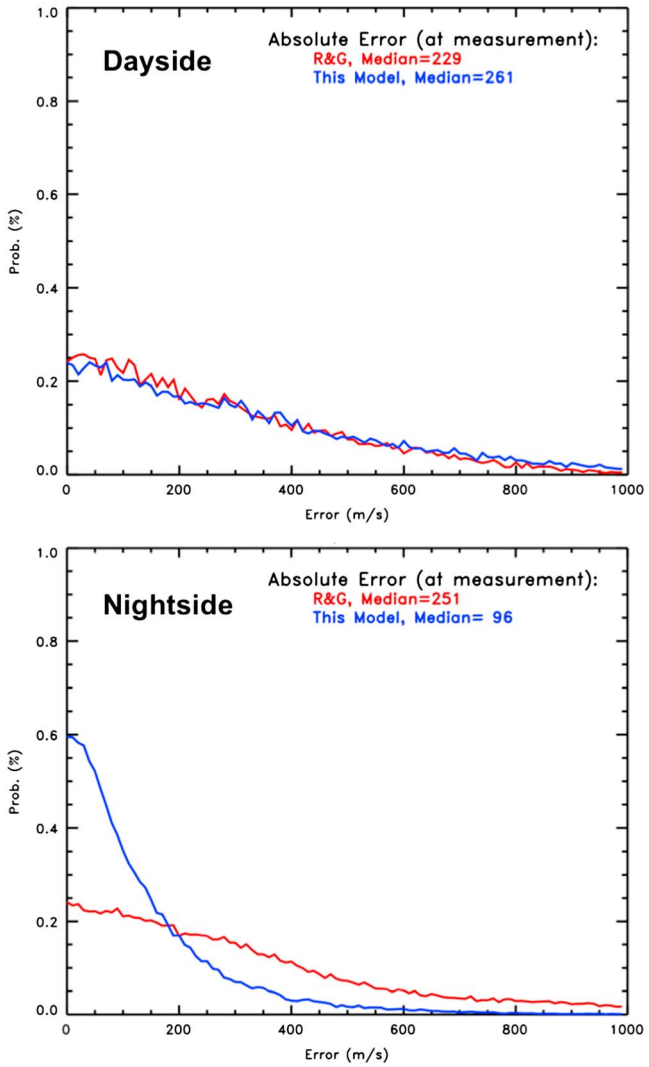

Figure 8. Absolute error between the final solution and the measured line-of-sight velocity components but only in the biteouts on the dayside and nightside. (top) Probability density function for absolute error in the dayside biteout for the R&G model (red) and this model (blue). (bottom) Same as top but for nightside biteout.

does not include any information regarding the state of the system and the internal M-I processes such as substorms (C and D). One might argue that this is implicitly included as certain driver conditions are more likely to be associated with such an internal M-I processes. However, this implies a third delay between the driver and the M-I response (e.g., substorm growth phase duration). Solar wind measurements directly upstream of the magnetopause are rarely available, and thus, we typically must assume that the measurements obtained at, for example, the L1 point are propagated correctly and are representative of what actually interacts with the magnetospheric field (E).

4.2.2. Using State Descriptors to Derive a Fill-in Model

By basing the model on a set of state descriptors, the assumptions of the cause and effect approach are avoided. This approach eliminates all five assumptions (A through E) listed above but introduces one new assumption: (A) The list of state descriptors is appropriate to describe the convection distribution.

It is not obvious that the ionospheric convection can be parameterized by a list of magnetic indices (and the SZA). However, the validation performed in section 4.1 provides support for this approach. In particular, Figure 7 shows that the PCR-based fill-in model is in significantly better agreement with the measured flows. On the dayside, it was expected that the IMF-driven model would be suitable since the electrodynamics are known to be largely directly controlled by the solar wind conditions.

4.2.3. Implications of the Different Techniques

In Figure 9 we showed the difference in the dynamic behavior of the two techniques. With the above assumptions in mind we can now interpret the implications of these differences.

In the RG&RB model the fill-in model is solely driven by the IMF orientation. Thus, if the IMF orientation changes from 1 min to the next so will the fill-in convection distribution. This implies an instantaneous response of the convection distribution without any delays. This is in fundamental conflict with any cause-and-effect since this inherently must include a delay. In the M-I system at least three delays are present following a change in the solar wind driver: (1) the initial response of the ionospheric convection, (2) a slower reconfiguration as the M-I system adjusts to the new driver conditions, and (3) loading-unloading sequence (e.g., substorms). While the first is on the order of a few minutes (e.g., Lu et al., 2002), the second may be 15–25 min (e.g., Ridley et al., 1999) and the growth phase of substorms is even longer. The RG&RB technique does not account for any delays.

In our technique we do not have any implicit information of the driver and thus neither do we have any information regarding delays between the driver and the effect. This may be inherently included as the magnetic indices are due to currents flowing in the M-I system that ultimately are driven by energy flowing from the solar wind into the M-I system.

With this in mind we expected that the IMF-driven fill-in model would outperform our model on the dayside but, surprisingly, Figure 7 shows that our model is in significantly better agreement with measurements than the RG&RB model. We speculate that this is due to the use of SuperMAG local time indices (sunlit and darkness auroral electrojet indices [SML/SMU] and local time ring current indices [SMR]), which apparently allows the model to reproduce the differences between nightside and dayside behavior.

In Figure 9 we find that our model is far less dynamic than the RG&RB model. We argue that this is due to the different assumptions on which these models are based. As the IMF conditions change the RG&RB model switches abruptly between discrete solutions, which effectively assumes that the M-I system has no inertia. Our model has inertia inherently included as the solutions are driven by the state descriptors.

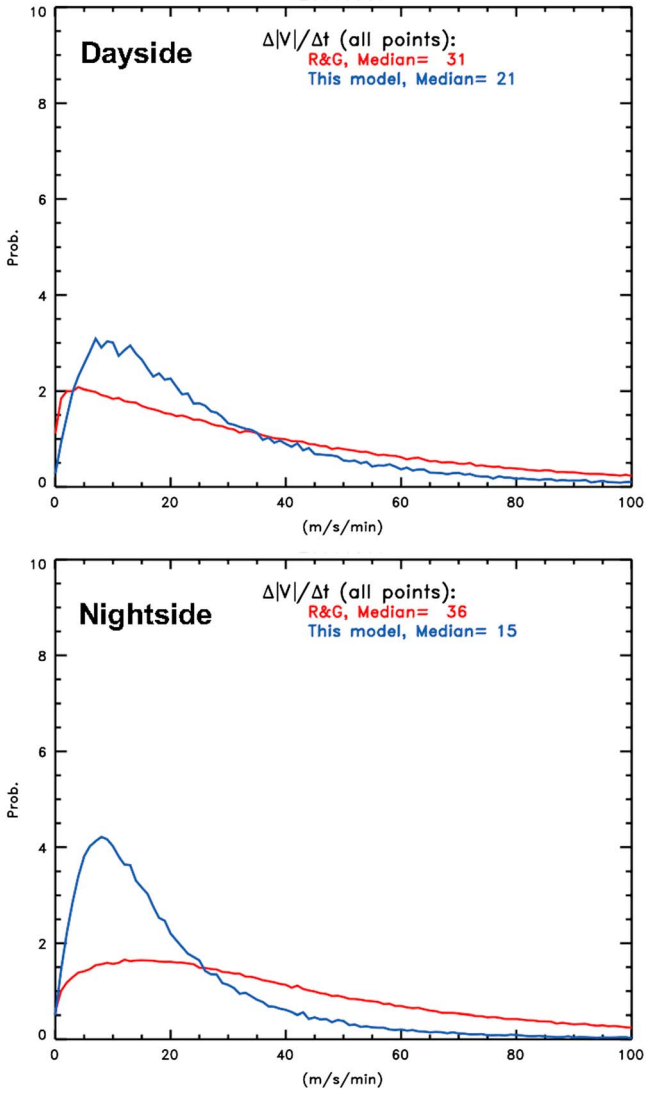

Figure 9. Change in speed of final solution. (top) Probability density function for absolute error on the dayside (06 to 18 magnetic local time) for the R&G model (red) and this model (blue). (bottom) Same as top but for nightside.

In conclusion, we emphasized that the question is neither whether IMF plays a role in controlling the ionospheric convection nor is it whether our state descriptors provide a complete description of the ionospheric convection. Rather, the question is to what extent these two fundamentally different techniques provide a means to derive the ionospheric convection. It is possible that a future iteration of our technique will include IMF with some appropriate delay included.

4.3. Mathematical Approach

In addition to the above mentioned philosophical differences between our technique and the standard technique there are a number of technical differences. For example, section 2.3 described how we derive the measured vector flow, $\overline{\boldsymbol{V}}_{SD}$, which differs from the standard approach.

4.3.1. Coordinate System

While magnetic coordinates are used to bin the LOS measurements, all analyses in the new PCR-model approach are completed in geographic coordinates. The advantage is that geographic (GEO) is an orthogonal coordinate system. The present SuperDARN processing transfers the data into AACGM after the location of the backscatter has been determined. There are consequences for transferring the data into the nonorthogonal AACGM coordinates.

The first involves the location of the data in this system and how spatial derivatives are computed. The correct mathematical approach in any nonorthogonal coordinate system is to use contravariant and covariant derivatives with the relevant Jacobian and metrics (e.g., Lysak, 2004; Proehl et al., 2002; Rankin et al., 2006; Waters & Sciffer, 2008). For AACGM coordinates, these metrics would need to be computed numerically as they change with location.

The second consequence involves treatment of vectors in a nonorthogonal coordinate system. Any vector is usually described by two orthogonal components in an orthogonal, two-dimensional system such as GEO (e.g., north, east). For a nonorthogonal AACGM 2-D surface (at constant radial distance), four vector component directions are available. These are the vectors parallel to the coordinate directions (e.g., magnetic north and east), which are nonorthogonal, and the two vectors that are perpendicular to these. The vectors used in the standard SuperDARN data processing transform the GEO Doppler velocity vectors into one component that is parallel with AACGM north-south (i.e., latitude), and the other is forced to be orthogonal to that, which is not parallel to the AACGM longitude. In fact, the variation between this vector component and the AACGM longitude varies with position. This complicates the interpretation of the actual ionospheric convection in real space. The new approach to SuperDARN data processing described in this paper avoids all these complications by using GEO vector data.

4.3.2. The Use of Spherical Cap Harmonics

In order to derive the final solution, a vector spherical cap harmonic solution is computed based on the measured vector flow, $\overline{\boldsymbol{V}}_{SD}$, and the fill-in vector flow, $\overline{\boldsymbol{V}}_{PCR}$.

It is important to note that our technique does not require the use of any spherical cap harmonics or other fitted solution in order to provide the ionospheric convection. However, for computing additional quantities such as the potential (voltage), a potential basis function expansion, as used in the present processing, can be applied. There is one significant difference between the present approach and the new PCR-based model. The standard SuperDARN technique utilizes the so-called Heppner-Maynard boundary. This allows the velocities to be set to zero below some low-latitude boundary. This is required in order to satisfy a boundary condition of the basis function expansion applied to the data. The procedure is described in detail by Shepherd

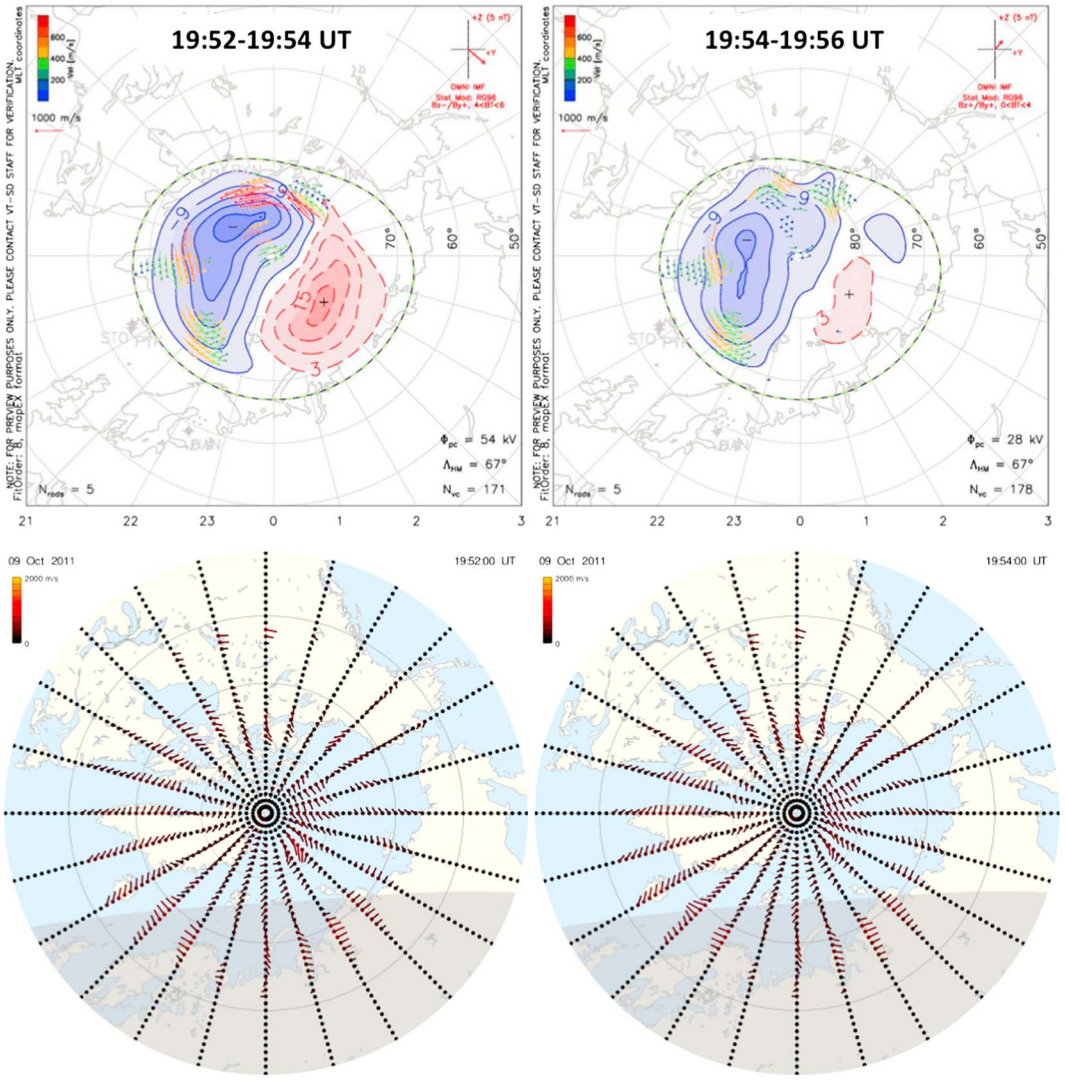

Figure 10. An example from October 9 2011 of Super Dual Auroral Radar Network convection patterns (downloaded from vt.superdarn.org) and our solutions for an abrupt change in the interplanetary magnetic field. Note that the rapid transition seen in the vt.superdarn.org solutions (flows as well as cross polar cap potential drop) are not reproduced by our model.

and Ruohoniemi (2000). This basic approach was first introduced by Ruohoniemi and Baker (1998), who used a circle at constant latitude. While equations 2 and 3 of that paper describe the use of spherical harmonic basis functions, equation 6 of the same paper specifies how these are distorted into functions that no longer have the properties of spherical harmonics. This is not a problem if the fitted data are derived from an expansion of the same distorted functions. However, this approach does require the unnecessary low-latitude zero velocity boundary condition. When the vector spherical cap harmonic basis functions are used, both Dirichlet and Neumann boundary conditions are available, allowing for nonzero values at the low-latitude boundary of the data. This is particularly important for including the data available from the increasing number of midlatitude radars in the network.

4.4. Spatiotemporal Resolution

The input data use the standard SuperDARN technique, which includes a so-called median filtering in step 2. This consists of deriving the median LOS flows in a grid that is 3 range-gates by 3 beams by 3 time steps. This implies that the temporal resolution of the resulting convection map is 6 min given the historical radar scan period of 2 min. The spatial resolution is 3 times the range gate resolution and 3 times the beam width. The

azimuth resolution is thus ~10° by ~150 km wide in the along beam direction. The median filtering includes three adjacent beams and thus three azimuths, which strictly speaking does not allow a simple median filtering since these point in three different beam directions. Future refinements of our technique can eliminate the need for the median filtering and thus minimize the smearing in space and time.

5. Summary and Conclusions

A new approach for determining the global ionospheric convection using SuperDARN measurements has been described. Our model avoids a number of difficulties and assumptions inherent in the present approach, and we argue that our model is a significant improvement over the standard SuperDARN approach (RG&RB) since:

1. We use an orthogonal coordinate system (geographic) instead of a nonorthogonal coordinate system (AACGM) (see section 4.3.1).
2. We use spherical cap harmonics instead of distorted basis functions (see section 4.3.2).
3. We eliminate the need for the so-called Heppner-Maynard boundary (see section 4.3.2).
4. We limit the set of inherent assumptions on which the fill-in model is based (see section 4.2.1).
5. We use the entire set of SuperDARN measurements (all northern stations and all years) to derive coefficients.

In addition to this list there are several other technical advantages to our approach (see sections 3 and 4). The assumed immediate cause and effect IMF dependence on ionospheric convection has been abandoned. By keeping to GEO coordinates, the interpretation of the velocity data in the new model is much clearer, avoiding complications of the representation of vector flows in the nonorthogonal AACGM coordinate system. We found that our solutions are far less dynamic than the standard SuperDARN solutions, which are interpreted as being due to the fact that the standard SuperDARN technique excludes M-I inertia and communication delays while it is inherently included in our approach. Rather, we argue that the M-I system has inertia that prevents the global convection from changing abruptly in response to an IMF change.

Appendix A

If only one component of the vector flow is known, we use the notation U. If both components are known, we use the notation $\overline{\boldsymbol{V}}$.

Notation

Parameter	Explanation
$\boldsymbol{U_{SD,LOS}}$	Component of vector flow, in the LOS direction, measured by SuperDARN, also referred to as SuperDARN LOS flow
$\boldsymbol{U_{PCR,a}}$	Component of vector flow, at azimuth a, derived from PCR model
$\overline{\boldsymbol{V}}_{\boldsymbol{PCR}}$	Fill-in vector flow derived from multilinear regression model
$\overline{\boldsymbol{V}}_{\boldsymbol{SD}}$	Measured vector flow derived from U_{SD} and $\overline{V}_{PCR}$
$\overline{\boldsymbol{V}}$	Final flow velocity derived from spherical cap harmonics fit to $\overline{V}_{SD}$ and $\overline{V}_{MLR}$

Acknowledgments
The authors acknowledge the use of SuperDARN data. SuperDARN is a collection of radars funded by national scientific funding agencies of Australia, Canada, China, France, Italy, Japan, Norway, South Africa, United Kingdom, and the United States of America. The first author further acknowledge NSF EarthCube award 1541009.

References

Baker, K. B., & Wing, S. (1989). A new coordinate system for conjugate studies at high latitudes. *Journal of Geophysical Research*, *94*(A7), 9139. https://doi.org/10.1029/JA094iA07p09139

Chisham, G., Lester, M., Milan, S. E., Freeman, M. P., Bristow, W. A., Grocott, A., et al. (2007). A decade of the Super Dual Auroral Radar Network (SuperDARN): Scientific achievements, new techniques and future directions. *Surveys in Geophysics*, *28*(1), 33–109. https://doi.org/10.1007/s10712-007-9017-8

Cousins, E. D. P., Matsuo, T., & Richmond, A. D. (2013). Mesoscale and large-scale variability in high-latitude ionospheric convection: Dominant modes and spatial/temporal coherence. *Journal of Geophysical Research: Space Physics*, *118*, 7895–7904. https://doi.org/10.1002/2013JA019319

Cousins, E. D. P., & Shepherd, S. G. (2010). A dynamical model of high-latitude convection derived from SuperDARN plasma grift measurements. *Journal of Geophysical Research*, *115*, A12328. https://doi.org/10.1029/2010JA016017

Fiori, R. A. D., Boteler, D. H., Koustov, A. V., Haines, G. V., & Ruohoniemi, J. M. (2010). Spherical cap harmonic analysis of Super Dual Auroral Radar Network (SuperDARN) observations for generating maps of ionospheric convection. *Journal of Geophysical Research*, *115*, A07307. https://doi.org/10.1029/2009JA015055

Gjerloev, J. W. (2012). The SuperMAG data processing technique. *Journal of Geophysical Research*, *117*, A09213. https://doi.org/10.1029/2012JA017683

Gjerloev, J. W., Hoffman, R. A., Ohtani, S., Weygand, J., & Barnes, R. (2010). Response of the auroral electrojet indices to abrupt southward IMF turnings. *Annales Geophysicae*, *28*(5), 1167–1182. https://doi.org/10.5194/angeo-28-1167-2010

Greenwald, R. A., Baker, K. B., Hutchins, R. A., & Hanuise, C. (1985). An HF phased array for studying small scale structure in the high-latitude ionosphere. *Radio Science*, *20*(1), 63–79. https://doi.org/10.1029/RS020i001p00063

Grocott, A., Milan, S. E., Imber, S. M., Lester, M., & Yeoman, T. K. (2012). A quantitative deconstruction of the morphology of high-latitude ionospheric convection. *Journal of Geophysical Research*, *117*, A05317. https://doi.org/10.1029/2012JA017580

Haines, G. V. (1985). Spherical cap harmonic analysis. *Journal of Geophysical Research*, *90*(B3), 2583–2591. https://doi.org/10.1029/JB090iB03p02583

Kim, H.-J., Lyons, L. R., Ruohoniemi, J. M., Frissell, N. A., & Baker, J. B. (2012). Principal component analysis of polar cap convection. *Geophysical Research Letters*, *39*, L11105. https://doi.org/10.1029/2012GL052083

Lu, G., Holzer, T. E., Lummerzheim, D., Ruohoniemi, J. M., Stauning, P., Troshichev, O., et al. (2002). Ionospheric response to the interplanetary magnetic field southward turning: Fast onset and slow reconfiguration. *Journal of Geophysical Research*, *107*(A8), 1153. https://doi.org/10.1029/2001JA000324

Lysak, R. L. (2004). Magnetosphere-ionosphere coupling by Alfven waves at midlatitudes. *Journal of Geophysical Research*, *109*, A07201. https://doi.org/10.1029/2004JA010454

Marquardt (1963). An algorithm for least-squares estimation of nonlinear parameters. *Journal of the Society for Industrial and Applied Mathematics*, *11*(2), 431–441. https://doi.org/10.1137/0111030

Newell, P. T., & Gjerloev, J. W. (2011). Evaluation of SuperMAG auroral electrojet indices as indicators of substorms and auroral power. *Journal of Geophysical Research*, *116*, A12211. https://doi.org/10.1029/2011JA016779

Newell, P. T., & Gjerloev, J. W. (2012). SuperMAG-based partial ring current indices. *Journal of Geophysical Research*, *117*, A05215. https://doi.org/10.1029/2012JA017586

Ponomarenko, P. V., & Waters, C. L. (2006). Spectral width of SuperDARN echoes: Measurement, use and physical interpretation. *Annales de Geophysique*, *24*(1), 115–128. https://doi.org/10.5194/angeo-24-115-2006

Ponomarenko, P. V., Waters, C. L., & Menk, F. W. (2007). Factors affecting spectral width of HF echoes from high latitudes. *Annales de Geophysique*, *25*(3), 675–687. https://doi.org/10.5194/angeo-25-675-2007

Proehl, J. A., Lotko, W., Kouznetsov, I., & Geimer, S. D. (2002). Ultralow-frequency magnetohydrodynamics in boundary-constrained geomagnetic flux coordinates. *Journal of Geophysical Research*, *107*(A9), 1225. https://doi.org/10.1029/2001JA000135

Rankin, R., Kabin, K., & Marchand, R. (2006). Alfvenic field line resonances in arbitrary magnetic field topology. *Advances in Space Research*, *38*(8), 1720–1729. https://doi.org/10.1016/j.asr.2005.09.034

Ridley, A. J., Lu, G., Clauer, C. R., & Papitashvili, V. O. (1999). Reply [to "Comment on "A statistical study of the ionospheric convection response to changing interplanetary magnetic field conditions using the assimilative mapping of ionospheric electrodynamics technique" by A.J. Ridley et al."]. *Journal of Geophysical Research*, *104*(A3), 4393–4396. https://doi.org/10.1029/1998JA900147

Ruohoniemi, J. M., & Baker, K. B. (1998). Large-scale imaging of high-latitude convection with Super Dual Auroral Radar Network HF radar observations. *Journal of Geophysical Research*, *103*(A9), 20,797–20,811. https://doi.org/10.1029/98JA01288

Ruohoniemi, J. M., & Greenwald, R. A. (1995). Observations of IMF and seasonal effects in high-latitude convection. *Geophysical Research Letters*, *9*, 1121–1124.

Ruohoniemi, J. M., & Greenwald, R. A. (1996). Statistical patterns of high-latitude convection obtained from Goose Bay HF radar observations. *Journal of Geophysical Research*, *101*, 21,743–21,763.

Ruohoniemi, J. M., & Greenwald, R. A. (2005). Dependencies of high-latitude plasma convection: Consideration of interplanetary magnetic field, seasonal, and universal time factors in statistical patterns. *Journal of Geophysical Research*, *110*, A09204. https://doi.org/10.1029/2004JA010815

Shepherd, S. G., & Ruohoniemi, J. M. (2000). Electrostatic potential patterns in the high latitude ionosphere constrained by SuperDARN measurements. *Journal of Geophysical Research*, *105*(A10), 23,005–23,014. https://doi.org/10.1029/2000JA000171

Waters, C. L., Gjerloev, J. W., Dupont, M., & Barnes, R. J. (2015). Global maps of ground magnetometer data. *Journal of Geophysical Research: Space Physics*, *120*, 9651–9660. https://doi.org/10.1002/2015JA021596

Waters, C. L., & Sciffer, M. D. (2008). Field line resonant frequencies and ionospheric conductance: Results from a 2-D MHD model. *Journal of Geophysical Research*, *113*, A05219. https://doi.org/10.1029/JA012822